RSC Advances

ROYAL SOCIETY OF CHEMISTRY

www.rsc.org/advances

Photoelectrochemical study on the electron transport and recombination kinetics in an urchin-like Zn/ZnO hierarchical nanostructure

Fei Wang [a,b], Yiqing Chen*[a], Chao Liu [a], Qilin Ma [a], Tian Zhao [a], Min Wang [a]

[a] School of Materials Science and Engineering, Hefei University of Technology, Hefei, Anhui, 230009, People' s Republic of China.

[b] School of Electronic Science and Applied Physics, Hefei University of Technology, Hefei, Anhui, 230009, People' s Republic of China

*Corresponding author:

Yiqing Chen*

School of Materials Science and Engineering, Hefei University of Technology.

No.193 tunxi Rd., Hefei City, Anhui Province, People's Republic of China, 230009.

TEL&FAX: +86 551 62901139

Email: chenyq63@126.com

Abstract: Electron transport and recombination kinetics in dye-sensitized solar cells (DSSCs) based on an urchin-like Zn/ZnO heterostructure are characterized by the intensity modulated photocurrent/photovoltage spectroscopy (IMPS/IMVS), as well, a dynamic IMVS model correlating to the unique urchin-like configuration is developed for the first time. Intriguingly, the photoanodes with different micro morphology and micro structure generated by tuning the annealing time, show significant discrepancies in electron transport, recombination and charge collection. The photoelectrochemical study reveals that the electron transport properties are closely related with ZnO /electrolyte/dye interface and the metal/metal oxide Schottky junction nanostructure.

Key Words: photoelectrochemical study, electron transport kinetics, dynamic IMVS model, heterojunction nanostructure, urchin-like Zn/ZnO

1. Introduction

Since the pioneering work by Grätzel and the co-workers in 1991, the dye-sensitized solar cells (DSSCs) have been considered as one of the most promising candidates for the renewable energy devices because of their high efficiency and low production cost.[1] As one of the materials earliest employed in DSSCs, ZnO was also initially used as a working electrode based on nanoporous semiconductors for this type of device. [2,3] ZnO has the similar energy band levels and band gap compared to TiO_2, but it has higher electron mobility, which benefits the electron transport.[4,5] However, in spite of a large variety of ZnO-based nanostructures (ie., nanowires,[6,7] nanoparticles,[8,9] porous films,[10] tetrapods,[11] hierarchical aggregates,[12,13] nanosheets,[14] etc.) the conversion efficiency is still lower than that for TiO_2-based cells. Therefore, many efforts have

been made to achieve the high-performance ZnO-based DSSCs. In order to improve the efficiency, the intense research interest has been focused on the design and synthesis of novel ZnO-based nanostructure composites in recent years.[15-24] There have been many works on the fabrication and properties of ZnO-based hierarchical structures, such as ZnO nanowires/ZnO nanoparticles,[15] ZnO/ZnS,[16,17] ZnO/TiO_2,[18,19] SiO_2/ZnO/TiO_2,[20] ZnO/ZnS_xSe_{1-x}/ZnSe,[21] ZnO/Nb_2O_5,[22] ZnO/SnO_2/ZnO,[23] etc. It has been proved that a rational design and precise control of the configuration and composition of ZnO-based DSSCs can effectively enhance the DSSCs performance and functionality. The origin is that the heterojunctions or energy barrier formed at the hierarchical interface can suppress the electron recombination and consequently improve the electron collection efficiency. Compared to ZnO nanowires, the urchin-like Zn/ZnO core-shell structure exhibited a superior photoelectrical response property and photoelectrochemical performance.[24]Thus, the photoanodes with such unique composite nanostructure could the applied in DSSCs or other kinds of solar cells.

As a powerful dynamic photoelectrochemical method, the intensity modulated photocurrent/ photovoltage spectroscopy (IMPS/IMVS) has been widely applied to study the charge generation and transport dynamics in DSSCs.[25-26] During IMPS/IMVS measurements, a small sinusoidal light perturbation, $I_{ac} = I_0\delta e^{-i\omega t}$, is superimposed on the background light intensity I_0, and the information on charge-transport dynamic characteristic under short-circuit and open-circuit is provided by the observed periodic response of the photocurrent and photovoltage to perturbation. It has been proved that the exhaustive IMPS/IMVS studies can provide basic physical and chemical mechanisms in DSSCs.[27-29]

In order to obtain the details of the charge transport properties in DSSCs, it is required to

build an appropriate theoretical model correlating to the unique device configuration for fitting the experimental results. Unfortunately, only few analytical IMPS/IMVS expressions have been reported to describe ZnO-based hierarchical structures in DSSCs or other kinds of solar cells.[30] In this work, we develop a theoretical IMVS model for an urchin-like Zn/ZnO hierarchical nanostructure which is composed of a core made up of a micrometer scale sphere-shaped metallic Zn and a shell made up of numerous radially protruding single-crystalline ZnO nanowires (NWs). The experimental IMVS responses are measured and well fitted to the analytical expressions of our model. Moreover, we study the influence of annealing time on the micro morphology and micro structure, as well as the influence of ZnO nanowire (NW) diameter on the electron transport properties such as electron lifetime and transit time, which are the essential parameters to the solar cells due to the fact that they will ultimately determine the power conversion efficiency. Owing to the truth that the electron processes such as generation and recombination occur primarily or exclusively at different interfaces, the study on the interface properties is crucial to the performance enhancement for solar cells. In short, the photoelectrochemical study on charge carrier processes can provide new insights in the mechanism understanding of charge transport and recombination in such a hetero nanostructure, so that the strategies to improve the power conversion efficiency can be formulated for solar cells.

2. Experimental Section

2.1 Synthesis and Device Fabrication.

3D urchin-like Zn/ZnO composite structure was synthesized by a method of thermal treatment. High purity Zn powder (2g, 99.999%, Aladdin) was mixed with the adhesive (containing 1ml acetylacetone, 1g ethylcellulose and 10ml terpineol), and the mixture was grinded

to form a slurry. Then the Zn powder slurry was coated evenly on the fluorine-doped tin oxide (FTO) glass cleaned by the ultrasonic, with the slurry thickness of about 20 μm and the area of 0.49 cm^2. The Zn powder slurry on the FTO glass was annealed in the furnace at 550 ℃ for 3 h, 6 h, 9 h, respectively, with the heating rate of 3 ℃min^{-1}. The furnace was then cooled to room temperature at the rate of 3 ℃min^{-1}.

To fabricate DSSCs, the FTO glass substrate was platinized on the conducting surface and was subsequently used as a counter electrode. The urchin-like Zn/ZnO electrode was immersed into a 0.3 mM N719 ethanol solution for 12 h to ensure the dye molecules adhere to the surface of ZnO film. Then the sample was rinsed in ethanol, and was dried in air. The sensitized photoanode and the counter electrode were separated and fixed by 25 μm Surlyn thermal-plastic spacer. Iodide-based electrolyte (3-methoxy acrylic nitrile/ionic liquid/GuSCN) was injected into the space between the two electrodes through a hole on the counter electrode fabricated in advance.

2.2 Characterizations and Measurements.

The morphology of the as-prepared urchin-like Zn/ZnO was characterized by a field emission scanning electron microscopy (FE-SEM, SU8020). High resolution transmission electron microscopy (HRTEM, JEM-2100F), selected area electron diffraction (SAED, JEM-2100F), and X-ray diffraction (XRD, D/MAX2500V) were used to characterize the microstructures and composition, respectively. The dynamic IMVS and IMPS measurements were carried out on the Zahner Zennium electrochemical workstation (Zahner Co., Germany) equipped with a frequency response analyzer. An intensity modulated blue light emitting diode (478 nm) driven by a source supply (Zahner) was used as the light source. The LED provided both dc and ac component of the illumination. The illumination was always incident on the working electrode side of the solar cell.

IMVS was performed under the open-circuit conditions, while IMPS was performed under the short-circuit conditions. The light intensity ranged from 100 to 180 Wm^{-2}. In the dynamic measurements, the small sinusoidal perturbation $I_{ac} = I_0\delta e^{i\omega t}$ was applied in the scanning frequency ranged from 10000 HZ to 100 mHz for both IMPS and IMVS. The sinusoidally-modulated light had a small ac component, which was 10% of the dc component.

3. Theory: the IMVS Model

Scheme 1 illustrates the cross-sectional structure of the cell device with a compact particle layer deposited on the FTO substrate. The particle has an urchin-like structure composed of numerous ZnO nanowires (NWs) protruding radially from the Zn sphere. The photo-induced electrons generated from the dyes are injected into the ZnO NWs, and subsequently diffuse along the axis direction of the ZnO NWs to the ZnO/Zn interface, then to the Zn core, and finally are collected by the FTO substrate. The unit cell and characteristic dimensions shown in Scheme 1 are used as the basis for the theoretical IMVS model, where *d* is the average length of ZnO NWs and *R* is the average radius of Zn sphere. As we known, if the light scattering is negligible, the exciton transport in the semiconductor photoanode under the steady-state conditions can be described by the standard diffusion equation.[25] If the time-dependent density of the photo-induced electrons at the location $(\rho - R)$ away from the Zn/ZnO interface where $(\rho = R)$ is $n(\rho, t)$, the continuity equation in terms of polar coordinates for the electron density $n(\rho, t)$ at the position (ρ, θ) under the illumination from the FTO side can be written as[25]

$$\frac{\partial n(\rho,t)}{\partial t} = I\alpha e^{-\alpha(\rho-R)} + D\frac{\partial^2 n(\rho,t)}{\partial \rho^2} - \frac{n(\rho,t)}{\tau_n} \quad (R < \rho < R + d) \qquad (1)$$

where α is the absorption coefficient, which is determined by the loading and extinction coefficient of the adsorbed sensitizer dye. I_0 is the incident light intensity corrected for the

reflection losses. *D* is the diffusion coefficient of electrons in ZnO, and τ_n is the mean electron lifetime.

In the region $0 < \rho < R$, the electron generation will not affect the transport dynamics so that the continuity equation for the electron density $n_1(\rho,\theta,t)$ can be expressed as

$$\frac{\partial n_1(\rho,\theta,t)}{\partial t} = D_1\left[\frac{1}{\rho}\frac{\partial}{\partial \rho}\left(\rho\frac{\partial n_1(\rho,\theta,t)}{\partial \rho}\right) + \frac{\partial^2 n_1(\rho,\theta,t)}{\rho^2\,\partial\theta^2}\right] - \frac{n_1(\rho,\theta,t)}{\tau_n} \quad (0 < \rho < R) \tag{2}$$

where D_1 is the diffusion coefficient of electrons in Zn. At the open circuit, we assume that no current leaves or enters the ZnO NWs at both the ZnO/Zn interface and the outermost ZnO/electrolyte interface. In this case, the boundary conditions can be written as

$$\frac{\partial n(\rho,t)}{\partial \rho}\Big|_{\rho=R} = 0 \tag{3}$$

$$\frac{\partial n(\rho,t)}{\partial \rho}\Big|_{\rho=R+d} = 0 \tag{4}$$

The time-dependent electron concentration $n(\rho,t)$ will be in the form of

$$n(\rho,t) = (Ae^{\gamma\rho} + Be^{-\gamma\rho} + Ce^{-\alpha\rho})\exp(i\omega t) \tag{5}$$

with the coefficients *A*, *B*, *C*, γ as follows:

$$A = C\frac{\alpha(e^{-\gamma d} - e^{-\alpha d})}{\gamma e^{\gamma R}(e^{-\gamma d} - e^{\gamma d})} \tag{6}$$

$$B = C\frac{\alpha(e^{\gamma d} - e^{-\alpha d})}{\gamma e^{-\gamma R}(e^{-\gamma d} - e^{\gamma d})} \tag{7}$$

$$C = \frac{\alpha I_0 \delta}{D(\gamma^2 - \alpha^2)} \tag{8}$$

By solving the equation (1) with the boundary conditions (3) and (4), the ac component ΔV_{oc} can be written as

$$U(\rho = R) \sim \Delta V_{oc} = \frac{\alpha I_0 \delta}{(\tau^{-1} + i\omega - D\alpha^2)}\left[1 + \frac{\alpha}{\gamma}\frac{\left(2e^{-\alpha d} - e^{\gamma d} - e^{-\gamma d}\right)}{\left(e^{\gamma d} - e^{-\gamma d}\right)}\right] \tag{9}$$

In order to extract the time constants from the IMVS response, it is possible to fit the real *re*(ΔV_{oc}) and imaginary *im*(ΔV_{oc}) parts of eq 9 with expressions

$$Re(\Delta V_{oc}) = \frac{F_1}{1 + (\omega\tau_n^{Re})^2} \tag{10}$$

$$\mathrm{Im}(\Delta V_{oc}) = -\frac{F_2 \omega \tau_n^{Im}}{1+(\omega \tau_n^{Im})^2} \quad (11)$$

here F_1, F_2 are the fit parameters and τ_n^{Re}, τ_n^{Im} represent the electron lifetime. Under the open circuit condition, τ_n^{Re} and τ_n^{Im}, which describe the modulation of $n(\rho = R)$, will only be influenced by electrons generated at the surface $(\rho = R)$. The obtained analytical results are in agreement with the previous reports, i.e., Schlichthörl G. etc.[27]

4. Results and Discussion

4.1 Micro morphology and Microstructure of the Urchin-like Zn/ZnO. Table 1 summarizes the synthesis conditions and morphology characteristics of the urchin-like Zn/ZnO films. Hereafter, the sample ID on the table will be used to identify the samples. For the characterization section, Fig. 2 shows the typical top-view SEM images of the as-synthesized urchin-like Zn/ZnO nanostructure on a FTO substrate. We can see that each urchin-like structure consists of numerous ZnO NWs protruding radially from the center of a sphere-shaped Zn core. The average diameter of the Zn core is 10~20 μm and the average length of ZnO NWs is ~10 μm. The length of the ZnO NW and the average diameter of ZnO NWs in urchin-like Zn/ZnO nanocture can be tuned by the annealing time. The morphology of urchin-like Zn/ZnO was obtained as shown in SEM images of Fig. 2. A large difference between S3 and S9 lies in the diameter of ZnO NWs. It can be seen that the diameter of ZnO NWs of S9 is much larger than S3, showing that the ZnO films of the urchin-like Zn/ZnO structure are growing thicker with increasing annealing time, due to the re-crystallization of ZnO NWs under high annealing time. As depicted in Fig. 3(a) and (b), the diameter of the ZnO NWs is almost increased with the annealing time, which is consistent with the results obtained from the SEM images. From the typical TEM images and SAED pattern of ZnO NWs scratched from the urchin-like Zn/ZnO framework S3 and S9 (inset, Fig. 3(a)-(c)), it

can be seen that the ZnO NWs are single-crystalline with a hexagonal wurtzite structure. The interplanar distance is 0.28 nm, confirming that the ZnO NW is grown with a preferential $(10\bar{1}0)$ orientation as indicated in Fig. 3(b). An XRD pattern acquired from the urchin-like Zn/ZnO sample clearly exhibits that the urchin-like structure is composed of Zn and ZnO. The curve is for ZnO NWs and Zn core, respectively, which corresponding to respective the typical diffraction peak of hexagonal Zn (JCPDS Card No.87-0713, a= 2.665nm, b= 2.665nm, c= 4.947nm) and hexagonal wurtzite ZnO crystal (JCPDS Card No.79-0206, a= 3.2499nm, b= 3.2499nm, c= 5.0266nm).

4.2 IMVS and IMPS. In order to gain into the charge recombination properties, the experimental IMVS responses are fitted with the calculated results using the analytical solution of eq10 and 11. Generally, the most satisfactory method to fit an IMVS response is to use its complex plane plot rather than its Bode form. We can see the experimental and the calculated IMVS responses of the as-prepared S3, S6 and S9 are all fitted very well as shown in Fig. 4 (a)-(c). The calculated electron lifetimes τ_n^{Re}, τ_n^{Im} and the fitted parameters F_1, F_2 are summarized in Table 2. It can be seen that the value of real part τ_n^{Re} is close to the imaginary part τ_n^{Im}. Additionally, the measured τ_n is close to the calculated τ_n^{Re} and τ_n^{Im}. The deviations of the calculated τ_n from the measured τ_n are only 6.7%, 7.8% and 8.3% for S3, S6 and S9, respectively. The satisfactory fits bear out that the IMVS theoretical model is consistent with the unique geometric configuration of the urchin-like nanoarchitecture. Fig. 5(a)-(c), the measured IMVS responses in Nyquist plot of S3, S6 and S9, showed a semicircle which was similar to previously reports by others[26]. Hence, the electron lifetime τ_n was directly obtained from the f_{min} point on the experimental IMVS response, using $\tau_n = {}^{1}/_{2\pi f_{min}}$. We can see a corresponding increase in f_{min} with the increase of ZnO NWs

diameter. To provide a clear presentation of the effect of ZnO NWs diameter on the electron recombination, the electron lifetime τ_n as a function of the ZnO NW diameter is illustrated in Fig. 5(d). As it is seen, the electron lifetime decreases with the increase of the ZnO NW diameter, showing that the electrons live shorter as the ZnO NWs grow thicker. In principle, electron recombination in DSSCs occurs at the interface between the semiconductor film and the electrolyte.[31] Nakade S. reported that the recombination lifetime decreased with the increase of TiO_2 nanoparticle size in DSSCs,[31] which is similar to our results. Thicker ZnO NWs mean the interfacial area is increased, which can lead to the increase of defect states and surface states, and then the increase of probability for electron recombination. What's more, several literatures studied the influence of annealing time on the structural and optical properties of Zn/ZnO films. In these studies, it was clearly observed that annealing time can change the surface structure and surface morphology significantly.[32-33] In our study, the samples with 3 h annealing time had the longest electron lifetime, 0.3s. The shorter τ_n of S6 and S9 may also be ascribed to the property that the crystallinity of ZnO NWS is decreased with the annealing time. The defects and surface states grow with the longer annealing time, leading to more electron recombination.

The measured IMPS responses in Nyquist plot for S3 and S6 are shown in Fig 6. (a) and (b). At short circuit, the measured electron transit time τ_d was directly obtained from the f_{min} point on the experimental IMPS response, using $\tau_d = {}^{1}/_{2\pi f_{min}}$. The increase of f_{min} with the increase of ZnO NWs diameter shows that electrons take shorter to reach the substrate. In general, the electron transit time τ_d depends on the ratio of free-to-trapped electrons and the diffusion coefficient of electrons in the conduction band[34]. τ_d reflects both of the electron transport and recombination processes. It can be clearly seen that the transit time of S3, 0.179s, is much longer

than S6. The decrease of τ_d with the increase of ZnO NWs diameter or the annealing time can be attributed to the fact that the electrons transport becomes more difficult as the increase of defect states. More defects make the increase of electrons loss in the transit process.

To investigate the effect of ZnO NWs diameter or the annealing time on the charge-collection efficiency, we can estimate it from the relation $\eta = 1 - \frac{\tau_d}{\tau_n}$. As shown in Table 3, electron transit time τ_d is smaller than electron lifetime τ_n, which is similar to the results from other groups[35]. It can be found that the charge-collection efficiency of S3 is 17% higher compared to S6, due to less electron recombination for S6. A Schottky junction is formed at the Zn/ZnO interface and the Schottky barrier can be in favor of the charge collection[15]. However, the surface states of the bulk semiconductor play a very important role in the Schottky barrier properties. Therefore, the different charge collection for S3 and S6 may be attributed to the discrepancy in their surface states. Faster recombination for thicker ZnO NWs significantly limits the charge collection process for solar cells. Moreover, relatively low collection efficiency can be attributed to the possibility that the diffusion length is not so long that a large number of electrons have been lost because of recombination process. Table 4 compares the *J-V* characteristics of the solar cells with the bare ZnO nanorods and S3 as the photoanodes respectively. Compared to the bare ZnO nanorods, the slightly increment in J_{sc} and η should be mainly attributed to the improvement in the charge collection efficiency due to the Schottky barrier formed at the Zn/ZnO interface. It is worth noting that the improvement of power conversion efficiency has not been so impressive, ascribed to truth that the problem of charge recombination at the ZnO/dye (or polymer) interface might be a more serious issue than electron transport in ZnO itself. Therefore, the recent application of ZnO based composite structures, e.g. a shell layer coated on ZnO may improve the

problem of interface recombination and enhance the power conversion efficiency.[36,37] In short, the power conversion efficiency is not so high for ZnO based solar cells may be ascribed to the relatively low charge-collection efficiency and serious problem of recombination at the interface. Therefore, the improvement of collection efficiency and interfacial modification become especially crucial to enhance the solar cell photoelectric performance.

5. Conclusions

In summary, this work presents a dynamic IMVS model for the urchin-like Zn/ZnO hierarchical nanoarchitecture in DSSCs, on the basis of the continuity equation for the density of mobile excess electrons. The fact that the measured IMVS responses are fitted well with the calculated ones proves the correctness of the theoretical model. The sample with 3 hour annealing time displays the longest electron lifetime, transit time and charge collection efficiency. An increased annealing time can change the micro morphology, microstructure and crystallinity of the urchin-like Zn/ZnO structure remarkably; as well the Schottky junction formed at the Zn/ZnO interface may affect the charge collection process. The photoelectrochemical study on charge carrier processes reveals that the electron back reaction in hierarchical nanostructure are concerned with the defect states, surface states and interface properties of the photoanodes, which can shed light on the charge transport and recombination kinetics in such core-shell structure. In order to gain outstanding micro parameters (such as electron lifetime, transit time, charge collection efficiency, etc.) and photoelectric properties, an optimized micro morphology and alternative interfacial modification both are proved to be very crucial to performance enhancement for solar cells.

Acknowledgments

This work was supported financially by National Nature Science Foundation of China (NSFC) (No.21071039).

References

(1) O' Regan, B.; Grätzel, M. Nature. 1991, 353, 737-740.

(2) Tributsch, H.; Gerischer, H. Phys. Chem. 1969, 73, 251-260.

(3) Tsubomura, H.; Matsumura, M.; Nomura, Y.; Amamiya, T. Nature. 1976, 261(5559), 402-403.

(4) Bauer, C.; Boschloo,G.; Mukhtar, E.; Hagfeldt, A. J. Phys. Chem. B. 2001, 105, 5585-5588.

(5) Katoh, R.; Furube, A.; Yoshihara, T.; Hata, K.; Fujihashi, G.; Takano, S.; Murata, S.; Arakawa, H.; Tachiya,M. J. Phys. Chem. B. 2004, 108, 4818-4822.

(6) Law, M.; Greene, L. E.; Johnson, J. C.; Saykally, R.; Yang, P. Nat. Mater.2005, 4, 455−459.

(7) Xu, C.; Wu, J.; Desai, U. V.; Gao, D. J. Am. Chem. Soc. 2011,133, 8122−8125.

(8) Saito, M.; Fujihara, S. Energy Environ. Sci.2008, 1, 280−283.

(9) Ambadea, S. B.; Mane, R. S.; Han, S.H.; Lee, S.-H.; Sung, M.M.; Joo, O.-S. J. Photochem. Photobiol. A. 2011, 222, 366−369.

(10) Yoshida, T.; Zhang, J. B.; Komatsu, D.; Sawatani, S.; Minoura,H.; Pauporte, T.; Lincot, D.; Oekermann, T.; Schlettwein, D.; Tada, H.; Wohrle, D.; Funabiki, K.; Matsui, M.; Miura, H.; Yanagi, H. Adv. Funct. Mater.2009, 19, 17−43.

(11) Chen, W.; Qiu, Y.; Zhong, Y.; Wong, K. S.; Yang, S. J. Phys. Chem. A. 2010, 114, 3127−3138.

(12) Zhang, Q. F.; Chou, T. R.; Russo, B.; Jenekhe, S. A.; Cao, G. Z. Angew. Chem., Int. Ed. 2008, 47, 2402−2406.

(13) Memarian, N.; Concina, I.; Braga, A.; Rozati, S. M.; Vomiero, A.; Sberveglieri, G. Angew.

Chem., Int. Ed. 2011, 50, 12321−12325.

(14) Lin, C.Y.; Lai, Y.H.; Chen, H.W.; Chen, J.G.; Kung, C.W.; Vittal, R.; Ho, K.C. Energy Environ. Sci. 2011, 4, 3448−3455.

(15) Puyoo, E.; Rey, G.; Appert, E.; Consonni, V.; Bellet, V. J. Phys. Chem. C. 2012, 116, 18117-18123.

(16) Chung, J.; Myoung, J.; Oh, J.; Lim, S. J. Phys. Chem. C. 2010, 114, 21360-21365.

(17) Saha, S.; Sarkar, S.; Pal S.; Sarkar, P. J. Phys. Chem. C. 2013, 117, 15890-15900.

(18) Xu, C. K.; Wu, J.M.; Desai, U. V.; Gao, D. J. Am. Chem. Soc. 2011, 133, 8122-8125.

(19) Wang, M. L.; Wang, Y.; Li, J. B. Chem. Commun. 2011, 47, 11246-11248.

(20) William, V. O.; Jeong, N. C.; Prasittichai, C.; Farha, O.K.; Pellin, J.P.; Hupp, J. T. ACS Nano. 2012, 6, 6185-6196.

(21) Wang, Z.; Yin, H.; Jiang, C.; Safdar, M.; He, J. Appl. Phys. Lett. 2012, 101, 253109.

(22) Ueno, S.; Fujihara, S. Electrochim. Acta. 2011, 56, 2906-2913.

(23) Chen, W.; Qiu, Y.; Zhong, Y.; Wong, K. S.; Yang, S. J. Phys. Chem. A.2010, 114, 3127-3138.

(24)Tang, D. M.; Liu, G.; Li, F.; Tan, J.; Liu, C.; Lu, G. Q.; Cheng, H. M. J. Phys. Chem. C. 2009, 113, 11035-11040.

(25) Dloczik, L.; Ileperuma, O.; Lauermann, I. ; Peter, L. M.; Ponomarev, E. A.; Redmond, G.; Shaw, N. J.; Uhlendorf, I. J. Phys. Chem. B. 1997, 101, 10281-10289.

(26) Schlichthörl, G.;Huang, S. Y.; Sprague, J.; Frank, A.J. J. Phys. Chem. B. 1997, 101, 8141-8155.

(27) Schlichthörl, G.; Park, N. G.; Frank, A. J. J. Phys. Chem. B. 1999, 103, 782-791.

(28) Guillèn, E.; Peter, L. M.; Anta, J. A. J. Phys. Chem. C. 2011, 115, 22622–22632.

(29) Lee, B. H.; Song, M. Y.; Jang, S. Y.; Jo, S. M.; Kwak, S. Y.; Kim, D. Y. J. Phys. Chem. C. 2009, 113, 21453–21457.

(30) Cui, Q.; Liu, C.; Wu, F.; Yue, W.; Qiu Z.; Zhang, H.; Gao, F.; Shen, W.; Wang, M. J. Phys. Chem. C. 2013, 117, 5626-5637.

(31) Nakade, S.; Saito, Y.; Kubo, W.; Kitamura, T.; Wada, Y.; Yanagida, S. J. Phys. Chem. B. 2003, 107, 8607-8611.

(32) Xiang, X.; Zu, X. T.; Zhu, S.; Wei, Q. M.; Zhang, C. F.; Sun, K.; Wang, L. M. Nanotechnology. 2006, 17, 2636–2640.

(33) Kuan, C. Y.; Hon, M.H.; Chou, J. M.; Leu, I. C. Growth Behavior, Cryst. Growth Des. 2009, 9 (2), 813–819.

(34) Peter, L. M.; Wijayantha, K. G. U. Acta. 2000, 45, 4543-4551.

(35) Park, N. G.; Schlichthörl, G.; Lagemaat, J. van de; Cheong, H. M.; Mascarenhas, A.; Frank, A. J. J. Phys. Chem. B. 1999, 103, 3308-3314.

(36) Li, Y.; Lu, P.; Jiang M.; Dhakal, R.; Thapaliya, P.; Peng Z.; Jha, B.; Yan, X. J. Phys. Chem. C. 2012, 116, 25248−25256.

(37) Xu, C.,; Wu, J.; Desai, U. V.; Gao, D. Nano Lett.2012, 12, 2420−2424.

Tables

Table 1 Preparation conditions and morphology characteristics of the urchin-like Zn/ZnO structure.

Table 2 The measured and calculated electron lifetimes τ_n and fitting parameters obtained for S3, S6 and S9.

Table 3 The measured electron transit times and collection efficiency obtained for S3 and S6.

Table 4 The photovoltaic characteristics (V_{oc}, J_{sc}, *FF*, and η) of photoanodes with bare ZnO nanorods and S3 under AM 1.5 G 1 sun (100mW/cm^2) illumination.

Table 1

sample ID	Annealing time, h	diameter of Zn core, um	length of ZnO NW, um	diameter of ZnO NW, nm
S3	3	10~20	~10	~30
S6	6	10~20	~10	~70
S9	9	10~20	~10	~90

Table 2

sample ID	measured τ_n	calculated τ_n		fitting parameters F_1	fitting parameters F_2
S3	0.30 s	$\tau_n^{Re} = 0.32s$	$\tau_n^{Im} = 0.37s$	6.01×10^{-4}	6.42×10^{-4}
S6	0.090 s	$\tau_n^{Re} = 0.083s$	$\tau_n^{Im} = 0.098s$	2.55×10^{-4}	2.49×10^{-4}
S9	0.012 s	$\tau_n^{Re} = 0.011s$	$\tau_n^{Im} = 0.013s$	3.83×10^{-5}	4.26×10^{-5}

Table 3

sample ID	electron lifetime τ_n	transit time τ_d	collection efficiency η_{cc}
S3	0.30 s	0.179 s	40.3%
S6	0.090 s	0.06 s	33.3%

Table 4

sample	V_{oc} (V)	J_{sc} (mA/cm^{-2})	*FF* (%)	η (%)
Bare ZnO nanorods	0.69	1.46	38.2	0.40
S3	0.58	1.88	46.8	0.51

Figure captions:

Scheme 1. Schematic diagram of the urchin-like Zn/ZnO for the dynamic IMVS model is in terms of polar coordinates and the coordinate $\rho = R$ indicates the ZnO/Zn interface.

Fig.2. FE-SEM images of the urchin-like Zn/ZnO hierarchical framework on FTO substrate prepared from different annealing times: (a)-(c) S3 with different scale bars; (d) S9.

Fig.3. (a) TEM image of ZnO NW scratched from S3. (b)-(c) ZnO NW scratched from S9: (b) TEM image; (c) HRTEM image Inset: SAED pattern; (d) XRD pattern of S9.

Fig.4. The measured and fitted IMVS responses of the urchin-like Zn/ZnO devices in complex plane plots as shown. The black solid curve and the red solid curve represent the calculated *Re(Voc)* and the *Im(Voc)*, respectively. The black cubes and the red arrows represent the measured *Re(Voc)* and the *Im(Voc)*, respectively. (a) S3; (b) S6; (c) S9.

Fig.5. The measured IMVS responses of the urchin-like Zn/ZnO devices in Nyquist plots with the red triangle identifying the f_{min} points. (a) S3; (b) S6; (c) S9; (d) Dependence of the electron lifetime on the ZnO NW diameter.

Fig.6. The measured IMPS responses of the urchin-like Zn/ZnO devices in Nyquist plots with the red triangle identifying the f_{min} points. (a) S3; (b) S6.

Fig.1.

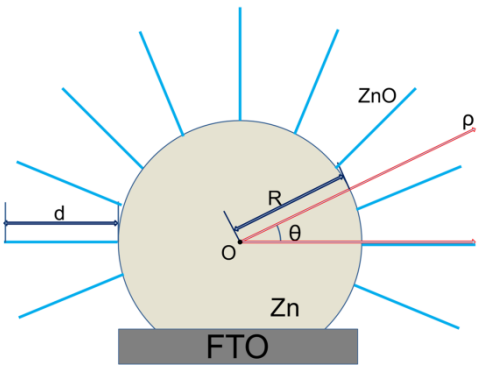

Fig.2.

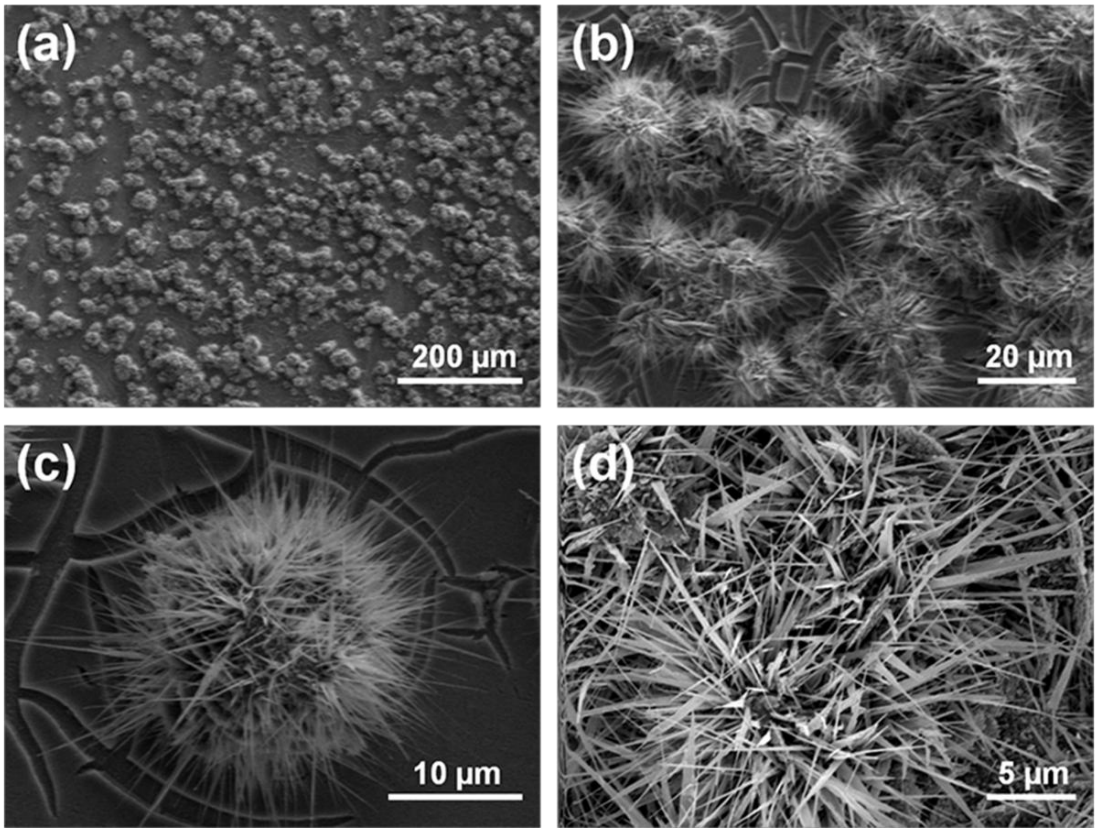

Fig.3

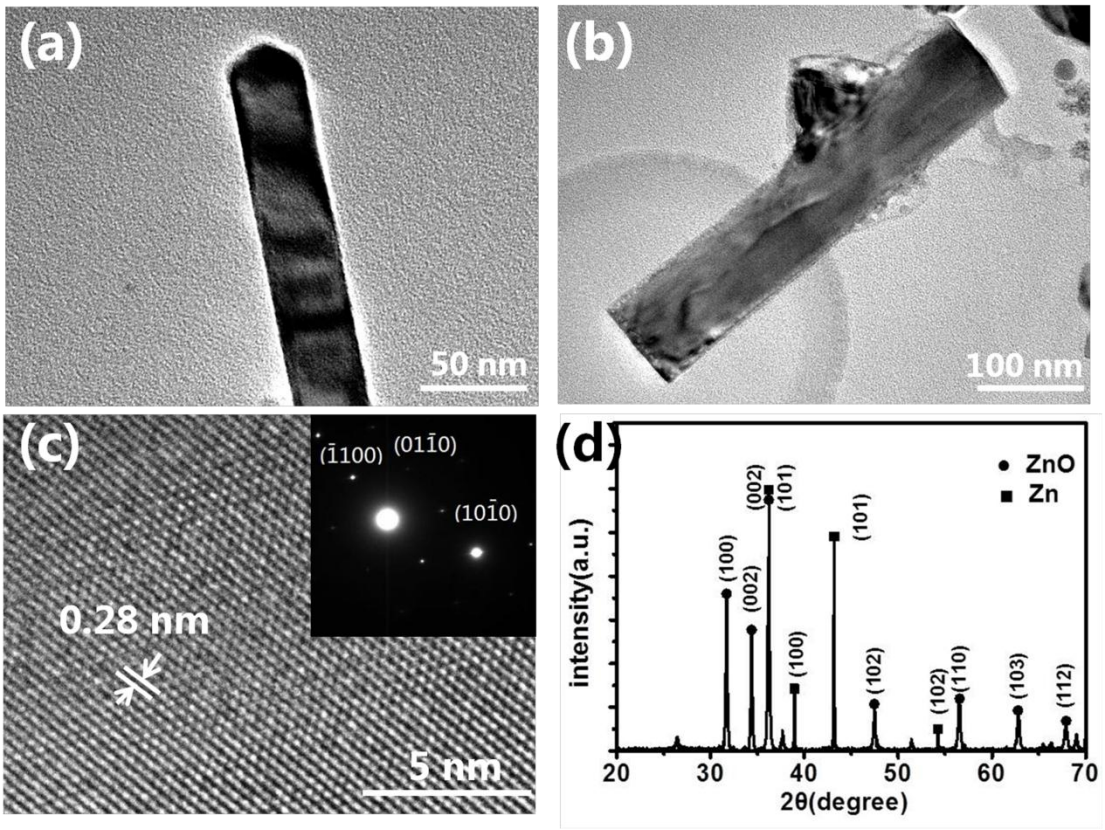

Fig.4

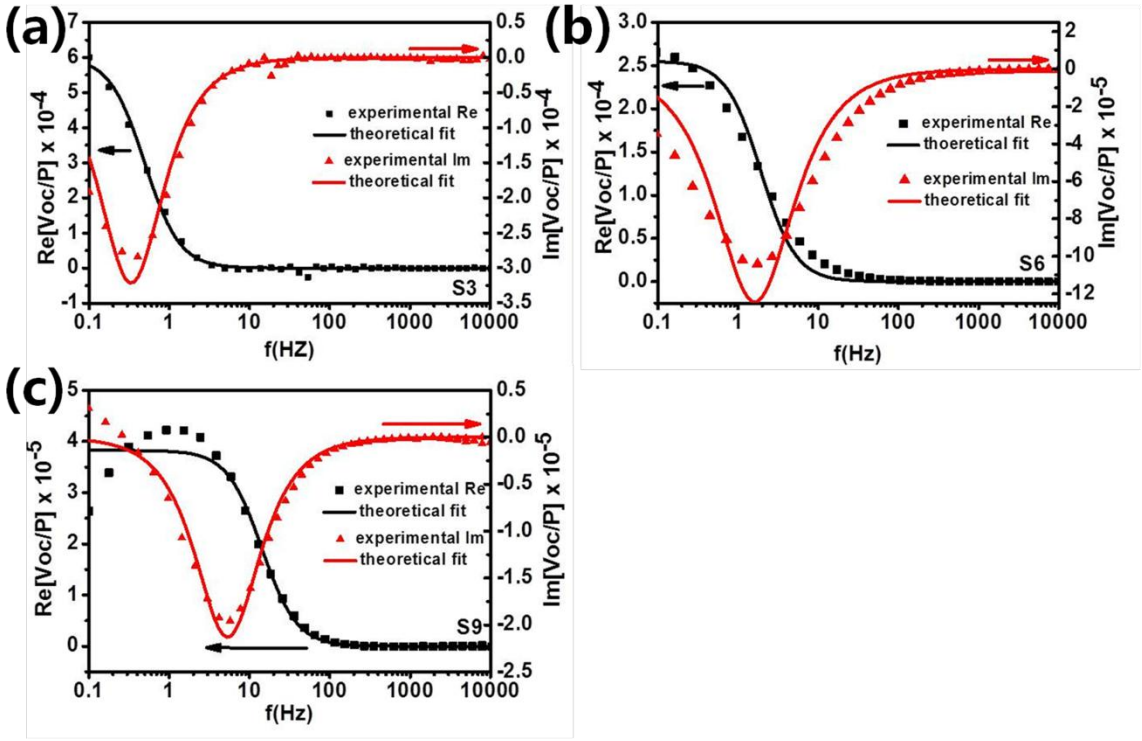

Fig.5

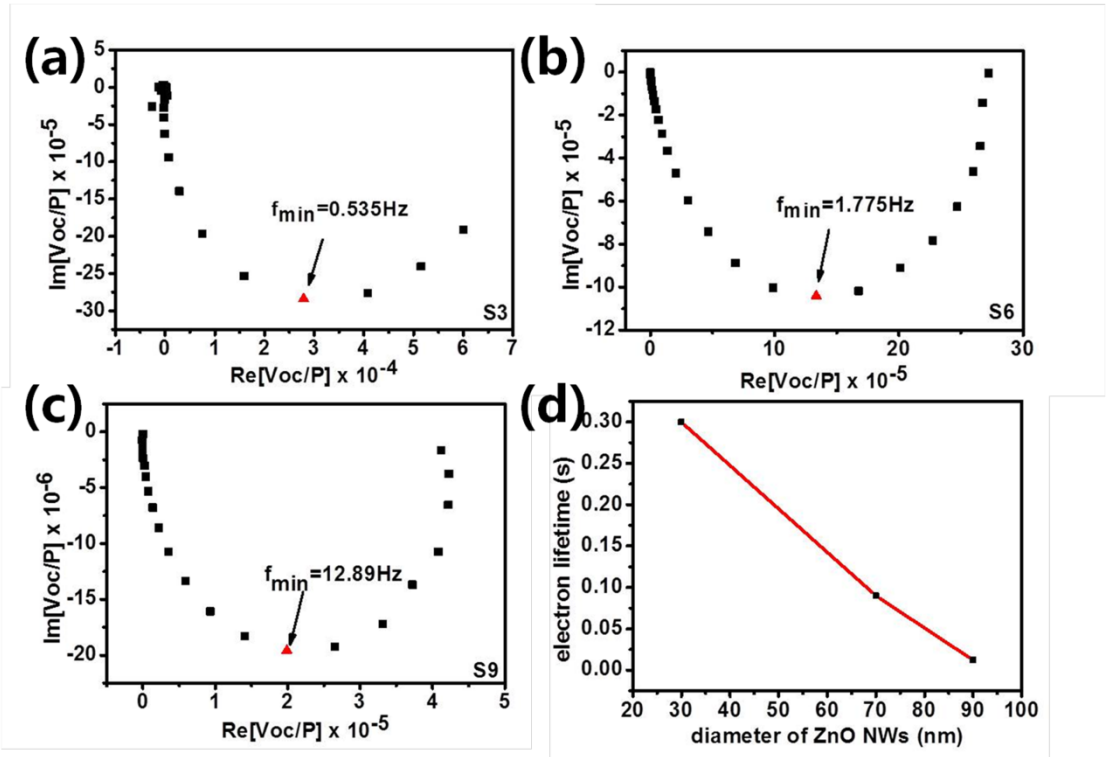

Fig.6